Torque Generation by the F$_o$ motor of the Sodium ATPase

Jianhua Xing,* Hongyun Wang,[†] Christoph von Ballmoos,[‡] Peter Dimroth,[‡] and George Oster*

*Departments of Molecular and Cellular Biology and Environmental Science, Policy and Management, University of California, Berkeley, California 94720-3112 USA; [†]Department of Applied Mathematics and Statistics, University of California, Santa Cruz, California 95064 USA; and [‡]Institute of Microbiology, Swiss Federal Institute of Technology, Zurich, Switzerland

ABSTRACT   Based on recent structural and functional findings, we have constructed a mathematical model for the sodium-driven F$_o$ motor of the F$_1$F$_o$-ATPase from the anaerobic bacterium *Propionigenium modestum*. The model reveals the mechanochemical principles underlying the F$_o$ motor's operation, and explains all of the existing experimental data on wild-type and mutant F$_o$ motors. In particular, the model predicts a nonmonotonic dependence of the ATP hydrolysis activity on the sodium concentration, a prediction confirmed by new experiments. To explain experimental observations, the positively charged stator residue (R227) must assume different positions in the ATP synthesis and hydrolysis directions. This work also illustrates how to extract a motor mechanism from dynamical experimental observations in the absence of complete structural information.

INTRODUCTION

In virtually every organism, ATP is manufactured by the enzyme F$_1$F$_o$-ATPase, also known as ATP synthase. The nomenclature refers to the two portions of the protein, both of which are rotary motors. The soluble F$_1$ portion contains the catalytic sites that synthesize, or hydrolyze, ATP according to the direction of rotation. The transmembrane F$_o$ portion normally generates the torque that is used by F$_1$ to pry the newly synthesized ATP from its catalytic sites. However, when the F$_1$ motor is in hydrolysis mode, it drives the F$_o$ motor in reverse to function as an ion pump. The F$_o$ motor is one of the two known molecular rotary engines that derive their energy from a transmembrane ion motive gradient (the other is the bacterial flagellar motor). In this article we present a new model for how the F$_o$ motor converts an ion gradient into a mechanical torque.

It is difficult to discern the operating principle of a device without knowing what it looks like. Thus a crucial step in understanding the operation of a protein is to obtain its molecular structure. Unfortunately, this is usually the most difficult step, especially for membrane proteins. It is easier to study the dynamical responses of the protein under various conditions such as substrate concentrations, the effects of mutations and, in the case of motor proteins, external loads. To unravel the workings of complex enzymes like the F$_1$F$_o$ ATP synthase, a multifaceted approach is necessary. Structural information gives only snapshots of the system in single (perhaps not native) states, biochemistry gives only average reaction rates, mutation studies identify crucial amino acids, and mechanical measurements define the range

of mechanical forces the protein can generate under different conditions.

Abstractly, the dynamical behavior of a system is governed by its free-energy profiles along some set of reaction and geometric coordinates. Thus theoretical studies frequently begin by constructing plausible free-energy functions and then comparing experimental observations with the dynamical behavior predicted by traversing the coordinates driven by these free-energy functions. In principle, this task can be carried out by molecular dynamics simulations; however, this requires accurate force fields, daunting computing resources, and the complete molecular structure. Here we illustrate an approach to modeling using the inverse procedure. We use incomplete available structural data to construct empirical free-energy profiles from experimental measurements. These are refined by adjusting structural dimensions to fit further experimental data. The method demonstrates how mathematical modeling can provide a way to combine structural information with biochemical, mutation, and mechanical measurements to elucidate the basic operating principles for a mechanoenzyme.

Most of the structural and functional studies of the F$_o$ motor have been performed on the enzymes from the bacteria *Escherichia coli* and *Propionigenium modestum*. The former is driven by a transmembrane proton motive gradient, whereas the latter is driven by a sodium electromotive gradient. The two types of motors are structurally similar in most respects, but with some notable differences. Here we focus on the sodium motor.

The F$_o$ motor is built from three different subunits, denoted *a*, *b*, and *c*, in the stoichiometric proportions ab_2c_α, where the value of $\alpha = 10-14$ is species dependent. The F$_o$ motor is conventionally divided into a ''stator'' (ab_2) and ''rotor'' (c_α) assembly, which counterrotates during normal operation. The rotor is built from a ring-shaped array of

double-helical c subunits that is attached to the central γ-subunit that acts as a shaft to transmit torque between F_o and F_1. The a subunit consists of at least five membrane-spanning α-helices; the coiled-coil b subunit homodimer connects the stator to the top of the catalytic hexamer of the F_1 motor (and, with the γ-shaft, transmits torque between the two motors). Fig. 1 illustrates various aspects of the structure.

SUMMARY OF EXPERIMENTAL RESULTS

Before describing the model, we summarize the experiments upon which the model will be built. The two-dimensional electron crystallographic model of the c oligomer shows that it consists of 11 double helices that assemble into two concentric rings (Fig. 1 b) (Vonck et al., 2002). Two helices from the outer ring and one from the inner ring form an aqueous half channel that is accessible from the cytoplasmic side. The Na^+ binding site on the rotor channel is located near the middle of the membrane, and is formed by E65 of one subunit and Q32 and S66 of a neighboring subunit (see Fig. 1, c and d). Sodium ions can access the middle of the membrane through these channels even in the absence of the stator (Meier et al., 2002; von Ballmoos et al., 2002a,b).

The transmembrane ion motive force is given by $\Delta\mu_{Na^+} = \Delta\psi + (RT/F)ln([Na^+]_p/[Na^+]_c)$, where ψ is the membrane potential, R the gas constant, T the absolute temperature, F the Faraday constant, and the subscripts "p" and "c" refer to the periplasm and cytoplasm, respectively. (Here we will refer to the side the rotor channels open into the cytoplasm, and the side the stator channel opens into the periplasm.) The Dimroth laboratory has performed extensive studies on the sodium-driven F_o motor to determine how F_o function depends separately on the two components of the ion motive force (Kaim and Dimroth, 1998a; Kluge and Dimroth, 1992; Wehrle et al., 2002). The results are summarized as follows.

$\Delta\psi$-Driven $^{22}Na^+$ uptake experiments show that the membrane potential is indispensable for motor rotation

F_o motors were reconstituted into liposomes containing no sodium ions, and the amount of $^{22}Na^+$ ions transported into the liposome was measured at various times after adding the $^{22}Na^+$ ions to the outside, both in the presence and absence of the membrane potential. Without the membrane potential, the motor did not rotate no matter how large the ion motive
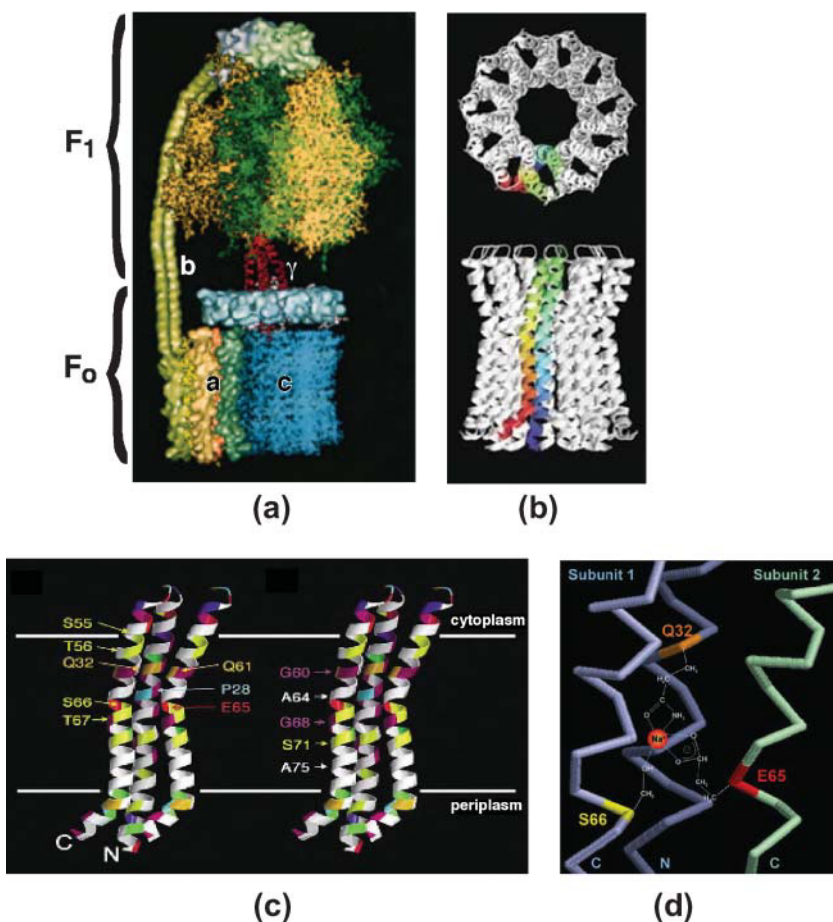

FIGURE 1 Structure of the F_o rotor and stator. (a) Overall structure of ATP synthase showing the F_1 and F_o motors connected by the γ-shaft and b subunits (from Pedersen et al., 2000). (b) Top and side views of the reconstruction of the c_{11} rotor (from Vonck et al., 2002). (c) Proposed residues comprising the rotor channel ion pathways (from Vonck et al., 2002). The rotor binding site is composed of residues E65, Q32, and S66. (d) Detail of the binding site showing the coordination of the sodium ion by the three residues (from Meier and Dimroth, 2002).

force. $^{22}Na^+$ accumulated inside the liposomes immediately after applying a membrane potential $> \sim 40$ mV. Rotation of the motor was confirmed by adding DCCD (a molecule that binds to the F_o rotor and sterically prevents it from completing a full rotation). In the presence of DCCD, $^{22}Na^+$ uptake was abolished. That the membrane potential is essential for rotation was further corroborated in ATP synthesis experiments with reconstituted F_1F_o-ATPase (Kaim and Dimroth, 1999; Kaim et al., 2002).

$Na^+/^{22}Na^+$ ion exchange measurements show that the ion channels are not voltage-gated

To test the possibility that the ion channels are voltage-gated, a series of $Na^+/$ $^{22}Na^+$ ion exchange measurements were carried out with no membrane potential. F_o motors were embedded into liposomes with Na^+ ions at various concentrations inside. $^{22}Na^+$ ions added externally accumulated in the liposomes, proving that the ion channels were not voltage-gated. Furthermore, the ion flux was bidirectional: each ion transported into the liposome was accompanied by an ion transported out. Therefore, no ion flux was observed if one side of the liposome contained no sodium ions. Ion exchange was not affected by adding DCCD, so full motor rotation was not a prerequisite of this process. These observations also demonstrated that there is no direct path for an ion through the membrane, and therefore the rotor channel must be closed on connecting to the stator channel.

F_o rotation driven by ATP hydrolysis rotation depends on Na^+ concentration

During ATP hydrolysis, the F_1 motor rotates in reverse, driving the F_o motor backward. This reverse rotation requires Na^+ ions, consistent with the ion-exchange experiments. Reverse rotation stopped if the triple mutation, aK220R, aV264E, and aI278N, was introduced to block the periplasmic stator half channel (see also Fig. 6) (Kaim and Dimroth, 1998a).

Stator mutants reveal the functional roles of the stator charge

A universally conserved arginine (aR227 in *P. modestum,* and aR210 in *E. coli*) is indispensable for maintaining the function of the F_o motor. To study the functional roles of this residue, Wehrle et al. (2002) performed the above-mentioned studies on F_o motors with mutant *a* subunits. Mutants with R227K and R227H retained considerable ATP hydrolysis-driven Na^+ transport activity, albeit at narrowed and somewhat shifted pH ranges. More strikingly, aR227A mutant without the positive charge was shown to catalyze ATP synthesis if the Na^+ concentrations were very low. In contrast to the wild-type motor, ATP hydrolysis-driven rotation of the aR227A mutant was not affected by the triple mutation (aK220R, aV264E, aI278N) (Wehrle et al., 2002). By comparing with

corresponding experiments on the wild-type motor, the essential feature of the residue aR227 is its positive charge. Structural information about the stator is based on the studies of the Fillingame group (Angevine and Fillingame, 2003; Angevine et al., 2003; Jiang and Fillingame, 1998).

Illustrations of the experimental setups are given in Fig. 2 and the experimental bases for the model are summarized in Table 1. The above experiments reveal a great deal of information about the rotor-stator interactions; they were used to construct the model. Next we develop a mathematical model that rationalizes all of these experimental observations.

THE MODEL

Constructing the model

An outline of the model construction procedure is as follows:

1. Reliable and generally accepted structural information was identified. For example, the rotor binding site lies close to the middle of the membrane.
2. From the structural information, the principal rotor-stator interactions were identified as electrostatic, hydration, and steric. The equations governing these interactions contained unknown parameters (e.g., dielectric constants) that were estimated from the experiments as follows.
3. The dynamical experiments provided qualitative information about the relative magnitudes of the rotor-stator interactions and greatly limited the possible values of the unknown parameters. This information was used to form a set of approximate free-energy profiles. Given the reliability of molecular motors under various environments and in the presence of Brownian motion, we assert that the dynamic properties of the motor are determined by the generic features of the free-energy profiles, rather than subtle details.
4. The approximate free-energy profiles were then fine-tuned by requiring the model to fit, simultaneously, all of the experimental data. Although there are quite a few parameters in the model, the model is not sensitive to most of them, and they are estimated based on physical considerations without further tuning. Only the strength and locations of the interactions are important for the dynamical behaviors of the model. These parameters were estimated first based on structural information and relevant physics, then fine tuned to fit experimental data quantitatively.
5. Predictions were made to test the model's validity. Certain structural conclusions can be drawn from the model. For example, the membrane potential must induce conformational changes in the position of the stator charge. This can be tested by i), examining the effects on motor function of cross-linking the stator helices, or ii), by NMR studies of the stator conformation as a function of membrane potential.
6. Once the final free-energy profiles were constructed, they were interpreted based on knowledge and/or inferences about the rotor and stator structure. For example, electrostatic interactions are expected between the stator charge R227 and the rotor sites. In the following discussion, we have used cartoon structures to aid in communicating the model. However, we emphasize that the model is independent of the details of these cartoon structures. For example, it is not important whether the stator has five or six transmembrane helices; the operating principle remains unaltered.

The important structural features in Fig. 1 are captured in the structural cartoon shown in Fig. 3. We model the rotor as a cylinder with 11 half channels equally distributed on the periphery. All 11 of the *c* channels are open to the cytoplasm when they are outside the *a-c* interface. To maintain
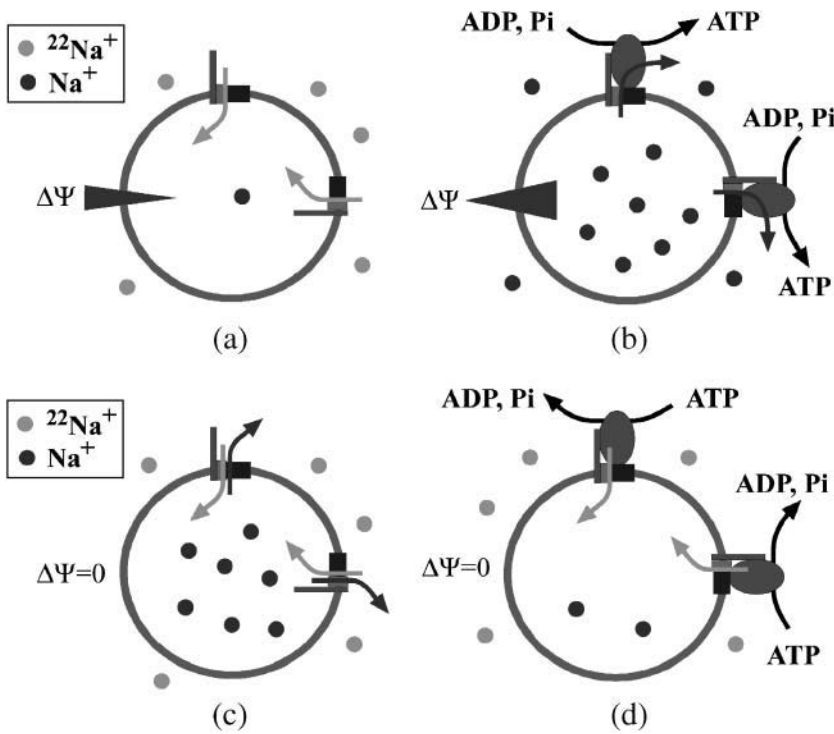
FIGURE 2 Experiments with radioactive ^{22}Na$^+$. (a) F_o-ATPase embedded in liposomes transports ^{22}Na$^+$ ions into the liposomes via rotation driven by the membrane potential. In the absence of the membrane potential, the motor does not rotate no matter how large the ion motive force. ^{22}Na$^+$ ions accumulate inside the liposomes immediately after applying a membrane potential $> \sim 40$ mV. Rotation of the motor was confirmed by adding DCCD, whereupon the $\Delta\psi$-driven ^{22}Na$^+$ uptake was abolished. (DCCD binds to the F_o rotor binding sites and sterically prevents it from completing a full rotation.) Upon adding F_1, the ^{22}Na$^+$ uptake rate was reduced by 50%, confirming that the F_o-ATPases are randomly oriented in the membrane. (b) Reconstituted F_1F_o-ATPase embedded in liposomes uses a sodium ion motive force, $\Delta\mu_{Na^+}$, to synthesize ATP. (c) Liposomes with F_o subunits randomly oriented have the capacity for ^{22}Na$^+$/Na$^+$ exchange in the absence of membrane potential. Liposomes are incubated with Na$^+$ ions inside. After adding ^{22}Na$^+$ ions outside, the ^{22}Na$^+$ uptake into the liposomes was measured. No ion exchange is observed without Na$^+$ ions inside the liposomes. Ion exchange is not affected by adding DCCD, so full motor rotation is not involved in this ion exchange. (d) Reconstituted F_1F_o-ATPase are embedded in liposomes. They pump ^{22}Na$^+$ ions into the liposomes when ATP is added to the outside and hydrolysis begins. The number of ^{22}Na$^+$ ions transported into the liposome was measured at various times after adding ATP.

the integrity of the stator against leakage, a rotor channel that lines up with the stator channel must be occluded (see below). The model parameters used in the simulations and data fits are summarized in Table 2.

For convenience of discussion, we divide the rotor-stator interface into three regions (see Fig. 3). Region 1 separates the stator channel from the outside lipid environment. Region 2 contains the aqueous stator channel where a sodium ion from the periplasmic side can bind onto a rotor site. Region 3 contains the stator charge whose electrostatic field affects the rotor site.

The mathematical model

To quantitatively fit data, we must cast the model as mathematical equations; these are described in the Appendix. In this section we outline how this was done.

averaged out). Therefore the motion of the motor is governed by a set of state-dependent potentials of mean force. Because of the rotational symmetry of the rotor, we need only treat explicitly the four rotor channels closest to the rotor-stator interface. These four sites can assume $2^4 = 16$ possible chemical states, denoted by s: (ion bound and nearly neutral, or not occupied and negatively charged). To model the ion exchange experiments, each site can be in 3 states: (empty, labeled occupied, and unlabeled occupied). Therefore, there are $3^4 = 81$ chemical states for the ion-exchange experiments. We measure rotation by the angle, θ, between the center of a rotor channel and the position of the stator charge; this coordinate system is shown explicitly in the Appendix. The dynamics of the motor is governed by a set of coupled Fokker-Planck equations that describe the evolution of the probability density, $\rho_s(\theta)$, of finding a rotor channel at position θ and chemical state s:

$$\frac{\partial \rho_s(t)}{\partial t} = -\frac{D}{k_B T}\frac{\partial}{\partial \theta}\left[\underbrace{\frac{\partial}{\partial \theta}\overbrace{\left(V_s(\theta) - \tau_L \times \theta\right)}^{\text{Motor and load torques}} \times \rho_s(\theta) + k_B T\,\overbrace{\frac{\partial \rho_s(\theta)}{\partial \theta}}^{\text{Rotor diffusion}}}_{\text{Rotor angular motion}}\right] + \underbrace{\sum_{s'}K_{ss'}(\theta)\,\rho_{s'}(\theta)}_{\text{Ion binding and release}}, \quad s = 1,2,\ldots,N. \tag{1}$$

The motion of the rotor is clearly the slowest degree of freedom. Therefore, we need treat explicitly only the rotation angle, θ, and the chemical states, $s_i = $ (ion bound, empty), of each $i = 1, \ldots, 11$ binding site. All other degrees of freedom settle to their equilibrium values so rapidly that they may be safely assigned their equilibrium values (i.e., Boltzmann

Here N is the total number of chemical states: 16 for normal operation, or 81 for ion exchange. D is the relative diffusion constant between the stator and the rotor, $\tau_L(\theta)$ is the load torque from F_1, and $K(\theta)$ is the Markov transition matrix between different chemical states. The forces between the rotor and stator are expressed in terms of the potentials of mean force, $V_s(\theta)$, when the

TABLE 1 Summary of experimental results and the implications for rotor-stator interactions

Experiments	Observations	Implications (based on observations in parentheses)
Ion exchange $\Delta\psi = 0$	1. Bidirectional flux requires ions on both sides of the membrane.	The potential for an empty state has barrier(s) bordering the stator channel region (from observation 1).
	2. Not affected by DCCD	The ion half channels are not voltage gated (1, 3, 4).
	3. Ion exchange at high (>1 mM) but not at low (≈ 10 μM) cytoplasmic Na$^+$ concentrations.	The rotor channel is closed on connecting with the a channel (1).
	4. Without stator charge: ΔpNa$^+$-driven uptake at low ((<0.1 mM) but not high (>1 mM) cytoplasmic Na$^+$ concentration.	Ion exchange by rotor rocking, not full rotation (2). Some potential barrier prevents the rotor from rotation (2). Stator charge affects ion affinity (3, 4).
$\Delta\psi > 0$	1. A membrane potential threshold of $\Delta\psi \sim -40$ mV is required for rotation.	A voltage-removable potential barrier prevents an empty rotor channel from diffusing between region 2 and 3 (1, 2).
	2. DCCD blocks rotation.	Given the small membrane potential threshold, effects of $\Delta\psi$ must be more than electrostatic interaction with the rotor sites (1).
	3. With stator charge: rotation with both high and low cytoplasmic Na$^+$ concentration.	Stator charge helps ion releasing to the cytoplasm (3, 4).
	4. Without stator charge: rotation only at very low cytoplasmic Na$^+$ concentration.	
ATP hydrolysis-driven rotation $\Delta\psi = 0$	1. With stator charge: rotation severely impeded when stator channel is blocked.	There is a high Coulomb potential barrier that prevents an occupied rotor channel from moving between region 2 and 3 (1, 2).
	2. Without stator charge: no effect, no Na$^+$ transport.	Stator charge helps ion releasing to the periplasm (1, 2).
	3. Require existence of Na$^+$	A rotor site needs to be occupied to enter the a-c interface through region 1 (3).

system is at position θ in the chemical state, s. Each potential has the following four contributions:

1. The electrostatic attraction between the positive stator charge and the negatively charged rotor sites, and the electrostatic repulsion between the positive stator charge and the positively charged ions occupying the rotor sites. For the A mutant, the stator charge is absent. This interaction was modeled by a screened Coulomb potential.
2. The interaction between the membrane potential and the rotor sites. Because of the nonuniform dielectric distributions along the rotation path, this depends on the rotational angle, θ.
3. The solvation energy of the rotor sites. This is largely due to formation of hydrogen bonds between water and polar residues when an empty site is in the stator half channel.
4. The steric interactions between the stator and the rotor—that is, those interactions that are independent of the chemical states of the rotor sites. This nonspecific interaction was modeled by a sine function with period equal to the distance between two neighboring rotor sites (Dimroth et al., 1999). This term is necessary to explain the experimental observation that the membrane potential and the ion concentration differences have different effects on motor rotations. This steric interaction term also helps prevent the rotor from slipping backward when working against a heavy load.

The Appendix provides all of the mathematical and computational details of the model construction.

The working principle of the wild-type motor

At physiological conditions, the motor torque is driven by the simultaneous interactions of two rotor sites with the stator in a ''pull-push'' mechanism

shown schematically in Fig. 4. A rotor site experiences two potentials, labeled ''Occupied'' when the site has a Na$^+$ bound, and ''Empty'' when the site is unoccupied. The ''Occupied'' potential is modeled as a dipole that corresponds to a (nearly) neutralized rotor site, whereas the ''Empty'' potential corresponds to a negatively charged site. The sodium binding site consists of three residues that combine to confer ion specificity. We model this as a single-shielded partial charge. The motor rotation is driven by diffusion and the combined electrostatic effects of the two rotor sites within the rotor-stator interface, the hydration of sites within the stator input channel, and the steric interactions between the rotor and stator. The sequence of events after the passage of a rotor site through the stator is described in Fig. 4. The actual potentials used in the model, as well as illustrations of the sequence of events, can be found in the movies in the Supplementary Material.

The membrane potential comes into play in two ways. First, it must move the stator charge several angstroms from its rest position to a position more advantageous for attracting the incoming rotor charge. This could be produced by a helical rotation of the α-helix driven by the membrane potential, analogous to the voltage-gated potassium channel. Second, if the stator channel is partially aqueous, then only a portion of the potential drop across the membrane will take place between the channel entrance to the middle of the membrane where the input channel terminates. The rest of the potential drop must occur horizontally between the end of the stator channel and the top of the rotor channel. This portion of the membrane potential contributes an electrostatic driving force to the motion of the rotor. In our model, 70% of the membrane potential drop is horizontal. In the kinetic model by Junge and co-workers, the horizontal component was put as high as 80% to fit their experimental data (Feniouk et al., 2004).

The process of moving the rotor one step (i.e., rotating $2\pi/11$) involves i), a ''power stroke'' corresponding to the electrostatic attraction between the stator charge and the empty rotor site and the torque due to the horizontal
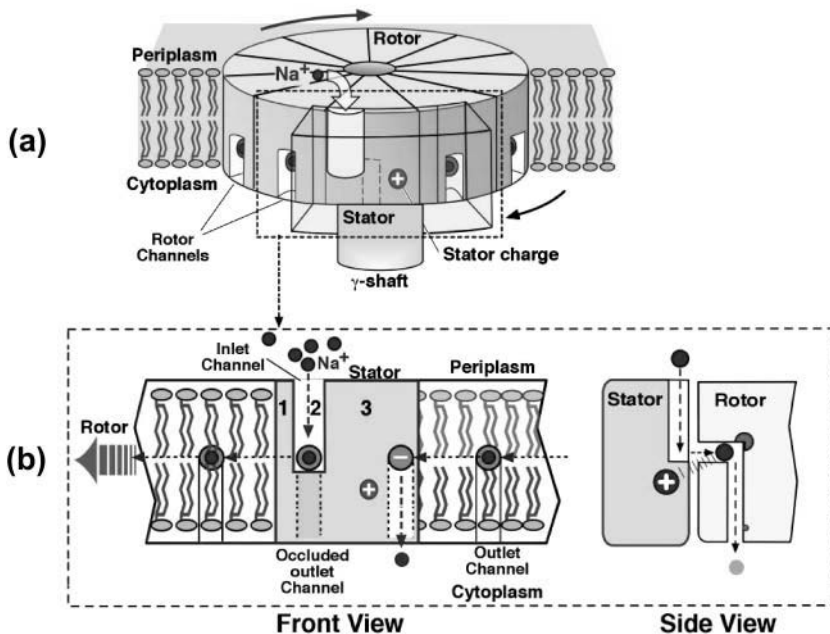
TORQUE GENERATION IN THE SODIUM F_o MOTOR

FIGURE 3 Cartoon structure (*panel a*) and front/side views (*panel b*) of the F_o rotor-stator assembly. The stator-rotor (*a-c*) interface is divided into three regions labeled *1*, *2*, and *3* (see *panel b*). In the ATP synthesis direction, a rotor site enters the interface from the right and, upon encountering the repulsive force from the positive stator charge in region 3, discharges its bound ion through the outlet channel to the cytoplasm. The rotor then diffuses carrying the site into the inlet channel (region 2), where it binds an ion from the periplasm. The nearly neutral site then leaves the interface through region 1. The inlet channel is connected to the rotor site via a short horizontal channel (*side view* in *panel b*), and the outlet channel is closed in region 2 to prevent ion leakage.

component of the membrane potential $(3\rightarrow4)$, and ii), a "ratchet" component corresponding to the hydration of the empty site in the input channel $(5\rightarrow6)$. The relative contribution of each to the total torque is computed by the mathematical model described in the Appendix using a numerical method similar to that described previously (Oster and Wang, 2003; Wang and Oster, 2001). This mechanism is different from that described in an earlier model (Dimroth et al., 1999), where the stator accommodated only one rotor site at a time. Recent electron cryomicroscopy studies show that the stator is large enough to span two rotor sites (Mellwig and Bottcher, 2003; Rubinstein et al., 2003).

In the ATP hydrolysis direction, the above process is reversed. To explain experimental observations, it is necessary to move the stator charge to a position closer to the stator channel than in the synthesis direction. This idea of two slightly different conformations for ATP synthesis and

hydrolysis was also suggested by Vinogradov (2000), and is consistent with the view that proteins are not rigid, but elastic, and deform oppositely when the direction of rotation is reversed. Compared to the synthesis direction, a stator charge closer to the stator channel is more effective in dislodging the bound ion of a rotor site incoming from region 1 through the stator channel. The movie provided in the Supplementary Material illustrates these points. Thus, as discussed above, the membrane potential plays dual roles: switching the stator charge position between the optimum for hydrolysis and synthesis, and helping to move an empty rotor site within the rotor-stator interface. These roles are easily realized due to the charge distributions and nonuniform dielectric distributions within the stator (Angevine and Fillingame, 2003; Angevine et al., 2003; DeLeon-Rangel et al., 2003). We note that, in the bacterial flagellar motor, the membrane potential is also necessary to maintain the functional motor conformation (Fung and Berg, 1995).

RESULTS

Torque generation for ATP synthesis

The first requirement for the model is that the F_o motor generate sufficient torque to release ATP from the F_1 catalytic sites during synthesis ($\sim$45 pN·nm). Fig. 5, *top panel*, shows that the model for the wild-type motor provides the necessary torque under experimental and physiological conditions. At low internal Na^+ concentrations (0.1 mM), the aR227A mutant motor also generates sufficient torque to drive ATP synthesis (Fig. 5, *bottom panel*). However, when the cytoplasmic Na^+ concentration is high enough to block the rotor channel, the motor is disabled. On the other hand, for the wild-type motor, the essential stator charge helps the rotor channel dislodge the ions inside the interface, and the motor works at both low and high Na^+ concentrations. Especially at physiological conditions with the cytoplasmic Na^+ concentration as high as 50 mM, the motor still rotates

TABLE 2 Parameter values used in the model

Parameter and units	Value
Diffusion constant of rotor, s^{-1}	5×10^3
pK_a of rotor sites	3.5
Radial coordinate of rotor binding sites, nm	2
z coordinate of rotor binding sites, nm	0
Radial coordinate of binding Na^+ ions relative to rotor sites, nm	0.3*, 0.1[†]
z coordinate of binding Na^+ ions relative to rotor sites, nm	0
Angular coordinates of binding ions relative to rotor sites	0*, 0.2 a_0[†]
Radial coordinate of the stator charge, nm	2.9 − 0.2 $f(\Delta\psi)$*, 2.7 + 0.3 $f(\Delta\psi)$[†]
Angular coordinate of the stator charge	−0.2 a_0 [1− $f(\Delta\psi)$]*, 0.15 a_0 + 0.5 a_0 $f(\Delta\psi)$[†]
z coordinate of the stator charge, nm	0.3 + 0.3 $f(\Delta\psi)$*, 0.5 + 0.3 $f(\Delta\psi)$[†]

*F_1F_o complex.
[†]F_o. The switching function $f(\Delta\psi)$ and a_0 are defined in the text.
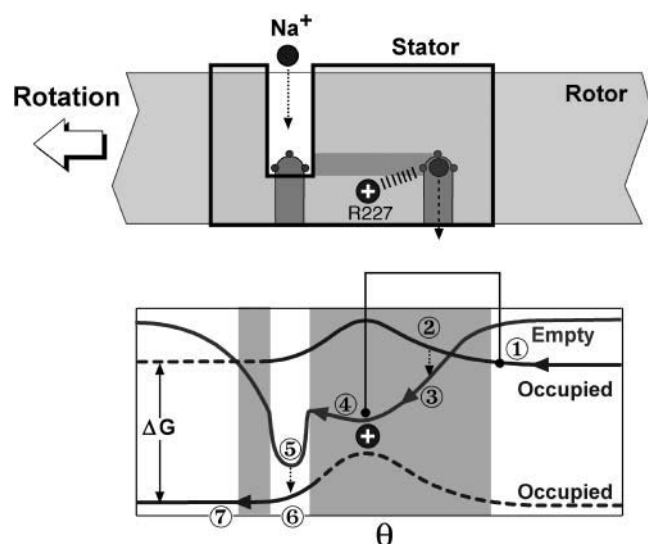
FIGURE 4 Operating principle of the F_o motor at physiological conditions. An occupied rotor site sees an Occupied potential, and an unoccupied site sees the Empty potential. An empty site lies in the Coulomb well due to the stator charge (*4*), and an occupied rotor site is about to enter into the *a-c* interaction region (*1*). The rotor diffuses until the left site moves into the input channel, where it solvates, preventing it from leaving the channel (*4→5*). This motion pulls the right-hand site into the *a-c* interface (*1→2*). The left site binds a sodium ion from the periplasm to be neutralized and switches to the occupied potential (*5→6*). Meanwhile, the right-hand site loses its ion to the cytoplasm and switches to the empty potential curve (*2→3*). The empty right-hand site is then pulled into apposition with the stator charge (*3→4*), and pushes the left-hand site out of the interface (*6→7*). After one cycle, the rotor site has carried an ion from the periplasm to the cytoplasm, resulting in a free-energy decrease $\Delta G = e\Delta\psi + k_B T \times ln([Na^+]_p/[Na^+]_c)$. The sodium ions lose free energy twice: once when binding to an empty site (*5→6*) and again when being released into the cytoplasm (*2→3*). Both events take place while the corresponding rotor sites interact with the stator and are torque-generating steps. Thus the Occupied potential for the rotor site emerging from the left side of the stator is ΔG lower than the Occupied site entering the right side of the stator.

at ~20 Hz. All these results agree with the experimental findings (Wehrle et al., 2002), and the estimated synthesis rate of *E. coli* and *P. modestum* (Kaim and Dimroth, 1999).

ATP hydrolysis and ion pumping

In hydrolysis mode, the F_1 motor drives F_o in reverse, and pumps ions from the cytoplasm side to the periplasm side. The mechanism of pumping can be understood by consulting Figs. 3 and 4, and the calculated results are shown in Fig. 6. A rotor site, loaded with a sodium ion, rotates to the right through region 1 into the rotor-stator interface. As it approaches the stator charge electrostatic repulsion dislodges the ion into the stator input channel. For the A mutant, a rotor site can be pulled through region 2 without releasing its binding ion. On the other hand, for a wild-type F_o motor, an occupied rotor is forced to give up its ion to the stator channel by the Coulomb repulsion between the stator charge
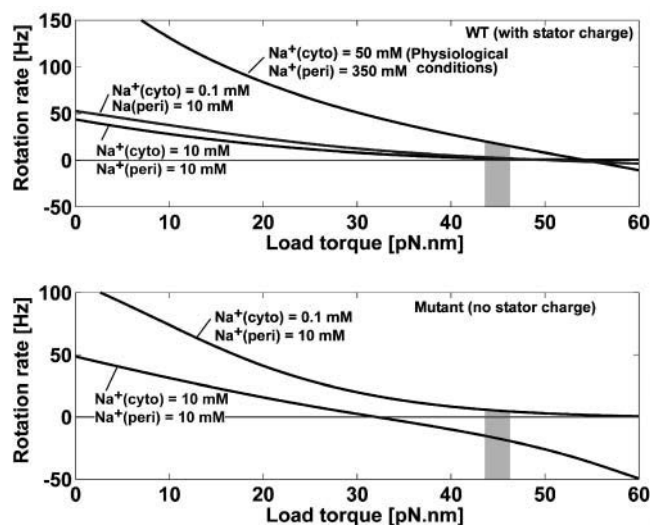
FIGURE 5 Torque generation (*Top panel*) The rotation rate of the wild-type as a function of the load torque. The membrane potential $\Delta\psi = -200$ mV. (*Bottom panel*) Same as top, for the A mutant.

and the binding ion. This scenario is consistent with experimental observations (Kaim and Dimroth, 1998a; Wehrle et al., 2002).

Laubinger et al. (1987, 1988) found that ATP hydrolysis requires the presence of Na^+ ions. The model predicts that the ATP hydrolysis rate increases with increasing Na^+ ion concentration, reaching a maximum at ~20 mM, then decreases at higher Na^+ concentrations. This prediction was
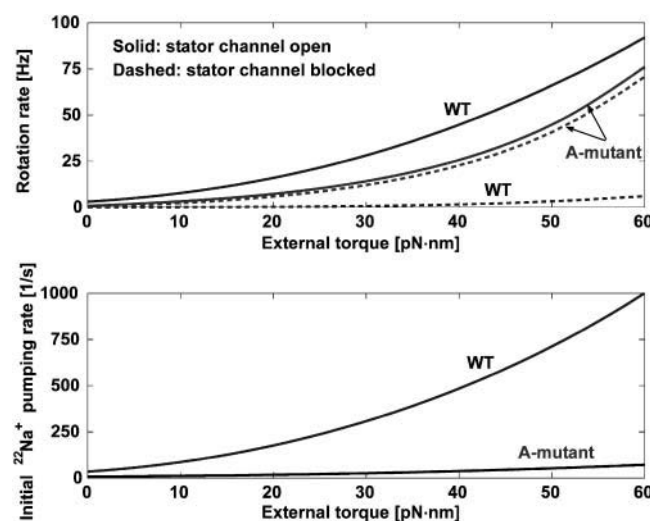

FIGURE 6 Hydrolysis. (*Top panel*) A triple mutation in the *a* subunit that blocks the stator channel severely impedes F_1-driven hydrolysis in the wild-type background (*solid line* versus *dashed line*), but has no effect on the A mutant type (*solid line* versus *dashed line*). (*Bottom panel*) Wild-type motor is efficient in pumping Na^+ ions since a rotor site must release its ion before leaving the stator channel; but in an A mutant, a rotor site can pass region 2 without releasing its bound ion. Thus it is an inefficient pump. In all calculations, Na^+ concentration in periplasm = 2 mM, Na^+ concentration in cytoplasm = 10 μM, and $\Delta\psi = 0$.

subsequently confirmed by experiments, as shown in Fig. 7; considering the experimental uncertainties, the agreement is remarkable.

In the Appendix we discuss further correspondences between experiment and computation of the F_o motor model in the synthesis and hydrolysis directions and in the idle state with no F_1 nor membrane potential. We also show that the operating principle of the sodium motor is nearly identical to its proton-driven counterpart.

General principles for F_o and V_o motors

This work has focused on the sodium F_o motor, and some subtle details may be specific only for this motor. However, from the model, one can infer some essential ingredients that would apply to the working mechanisms of F_o and V_o motors in general:

1. Solvation energy (i.e., formation of hydrogen bonds with water). The existence of hydrophilic ion channels lowers the free energy of empty rotor sites and restricts their motions inside the rotor-stator interface ensuring that only occupied states can escape. By coupling with the difference in ion concentration across the membrane, the solvation energy serves as a ''ratchet'' potential to bias the motor motion. Without the solvation energy term, the motor can still rotate at small loads, but cannot generate sufficient torque to release ATP from the catalytic sites of F_1. Existence of this solvation energy term is consistent with the conclusion of Junge and co-workers in their theoretical study of the two-channel proton F_o motor model (Cherepanov et al., 1999; Feniouk et al., 2004). To fit experimental data, they found that the pKa of the rotor site in the periplasm half channel must be smaller than that in the cytoplasm half channel.
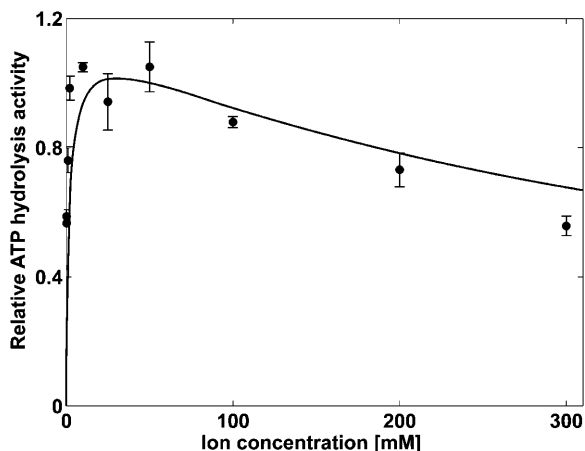

FIGURE 7   Sodium dependence. The ATP hydrolysis activity of the F_1F_o complex as a function of the Na^+ concentration ($C_p = C_c$) with no membrane potential. The solid circles are experimental data and the curve is the computed prediction of the model.

2. The stator charge. The positive stator charge ensures the dissociation of ions from an approaching rotor site, so the motor can function at physiological ion concentrations. In synthesis direction, it pulls an empty rotor site into the periplasm channel region, and discourages an occupied rotor site within the periplasmic channel from slipping through the Coulomb repulsion between the stator charge and the binding ion. In the hydrolysis direction, the Coulomb repulsion between the stator charge and the binding ion prevents a rotor site from moving out of the periplasmic channel without releasing the binding ion (Grabe et al., 2000).

3. Vernier mismatch. Because the elastic load from the F_1 portion of the protein always resists rotation, it is crucial that the F_o motor has a high duty cycle to avoid back slip. The solvation ratchet helps prevent reverse rotation. To ensure continuous forward rotation the power stroke of each rotor site must commence, or overlap with the end of the preceding rotor site's power stroke. We expect this feature to be true in general for ion-driven motors, including the bacterial flagellar motor (Berg, 2003). On the other hand, an ion-pumping motor, such as the V-ATPase, would operate more efficiently with fewer rotor sites, so that the torque from the V_1 ATPase needs work against the resistance of only one rotor site at a time (Grabe et al., 2000). These may explain why the c subunit stoichiometries of the F- and V-ATPases differ.

Comparison with the proton motor

Several structural features of the sodium F_o motor may differ from the proton drive counterpart, but definite answers require a high resolution structure of both. Despite these differences, the basic torque generating principle is the same in both motors. Here we briefly compare the two motors and comment on the differences between models.

According to these models, the most striking difference between the proton- and sodium-driven motors is the structural differences between their rotors and stators. The sodium motor has a single input half channel from the periplasm, and the 11 exit channels are located on the rotor. In the proton motor, the rotor sites are thought not to have access to the cytoplasm; rather a single half channel in the stator connects to the cytoplasm and provides the exit path for the occupied rotor sites as they enter the rotor-stator interface. (The differences in the number of c subunit double α-helices comprising the rotor are not significant with respect to the motor operation.) However, this is not as significant a difference as first appears because, at physiological conditions, sodium ions rarely dissociate into the cytoplasm until they complete a full rotation, enter the rotor-stator interface, and are dislodged by the stator charge. Thus the rotor half channels entering the stator play the same role as the permanent exit half channel in the stator of the proton

motor. The model presented here can be easily transformed to a two-channel model by allowing ion access to the cytoplasm only within a narrow range inside region 3 of the stator. Calculations show that the rotation rates are nearly indistinguishable.

One other difference is structurally significant. The rotor binding sites in the sodium motor (E65, Q32, and S66) are sequestered away from the rotor-stator interface (see Fig. 1 c), but the ions from the stator half channel need a pathway to the rotor sites. We propose a short horizontal channel connects the stator channel and the rotor binding sites (see Fig. 3 b). At the same time, the rotor channel to the cytoplasm must be sealed to prevent ion leakage. The mechanism for sealing off the rotor exit channel when it apposes the stator input channel may be that the rotor channels outside the interface have their fatty acid chain methylene groups on the outside. In the interface, however, the outside is covered by amino acid chains from the a subunit, which are much larger and could be sufficient to induce small conformational changes to block the channel.

Another mechanism was proposed for the proton motor: the binding site is presented to the rotor-stator interface via a helical rotation of the apposing c subunit. Our model cannot distinguish between these two possibilities (Angevine and Fillingame, 2003; Angevine et al., 2003; Dmitriev et al., 1999; Rastogi and Girvin, 1999). The sodium c subunit is expected to be less flexible than the corresponding proton subunit because Na^+ ions bridge neighboring c subunits, which stabilizes the c ring (Meier and Dimroth, 2002). On the other hand, the proton motor may experience larger thermal fluctuations that permit the outer c subunit helix to swivel outward as it enters the rotor-stator interface to present the proton binding site to the stator input channel (Angevine and Fillingame, 2003; Angevine et al., 2003; Dmitriev et al., 1999; Rastogi and Girvin, 1999). When out of the rotor-stator interface, the charge is sequestered inside the rotor away from the low dielectric environment of the membrane interface, with no access to the cytoplasm. However, because the timescale of the helical rotation is much faster than the rotation of the rotor, these motions do not enter into torque generation, and can be averaged out in the model. That is, the rotor-stator charge interactions should be understood as a potential of mean force, which is obtained by averaging out the fast fluctuations at each rotational angle.

An explicit model was constructed recently that includes rotations of the α-helices that ferry the protons through the rotor-stator interface (Aksimentiev et al., 2004). This model reveals more details of the process, and provides another way of constructing free-energy profiles by obtaining some parameters from molecular dynamics simulations. (In our work, all the interactions were identified and quantified from experimental data). The helical motions they consider take place on a timescale much faster than rotor rotation. Therefore, although these details may have biochemical significance (e.g., the path for ion access to the rotor site),

they can be Boltzmann averaged out, and will affect only the fine structure of the free-energy profiles. This is the standard adiabatic approximation in the theory of chemical dynamics. The basic operating principle revealed by the two models is essentially the same. If the helical motions are not fast enough, and there is memory effect, the F_o rotation rate can be enhanced, according to the Grote-Hynes theory (Grote and Hynes, 1980). This secondary effect does not change the basic picture presented by our model and the kinetic model of Junge and co-workers (Feniouk et al., 2004).

The existence of the membrane potential threshold for the proton motor is still controversial (Gräber et al., 1977; Junge, 1970, 1999; Kaim and Dimroth, 1999; Schlodder et al., 1982; Schlodder and Witt, 1980, 1981). However, our model posits that a major function of the membrane potential is to move the stator charge between two positions. The requirement of different conformations for the synthesis and hydrolysis functions was also suggested by others (Gräber et al., 1977; Schlodder et al., 1982; Schlodder and Witt, 1980, 1981; Vinogradov, 2000).

In the Appendix we discuss the relationship between the Markov/Fokker-Planck model developed here to purely kinetic models that have been used to model the proton F_o motor.

CONCLUSIONS

The model for the F_o motor presented here was developed by reconstructing the rotor-stator interaction components from experimental observations. The model provides a mesoscopic mechanism by which a transmembrane electrochemical gradient is converted into a rotary torque. This mechanism is a combination of Brownian ratchet and power stroke, and may apply more generally to all F_o motors of F_1F_o-ATPases (Oster and Wang, 2003; Wang and Oster, 2001).

Although the model presented here shares some features with previous models (Dimroth et al., 1999; Elston et al., 1998), it differs in several crucial aspects: two rotor sites occupy the rotor-stator interface, the stator charge moves under the influence of the membrane potential, and the accounting for the steric effect of the rotor shape. These features allow the model to explain all the experimental data at physiological ion concentrations, which previous models cannot. Thus a distinguishing feature of the model is that each assumption introduced is necessary to explain a particular set of experiments. The model results were subsequently verified experimentally, and others are readily testable.

Finally, the methodology of constructing empirical free-energy profiles step by step using incomplete information revealed by individual experiments should prove useful in modeling other protein motors. The model easily accommodates further quantification and adjustment when more experimental data on the sodium F_o motor becomes available. Especially important would be measurements of transient dynamics and mechanical measurements.

APPENDIX

Here we supply more detailed information about the model construction and numerical calculations.

Geometric setup for the model

The a subunit has five transmembrane α-helices (TMH). (There is some evidence for six TMH; however, we shall assume five. The pump's operating principle is the same in either case.) To form a stable structure, the helices are expected to arrange in two rows as shown in Fig. 8 a. The TMH containing R227 is placed in the middle of the first row facing the rotor. This is also consistent with the structural findings of the proton motor where two aqueous accessible half channels are found on the two sides of TMH IV containing R210 (Angevine and Fillingame, 2003; Angevine et al., 2003).

A side view of the motor is shown in Fig. 8 b. The rotor is modeled by a disk, so a cylindrical coordinate system is used with the origin at the center of the rotor. The periplasm stator channel divides the rotor-stator interface into three regions; the geometric parameters characterizing the rotor and stator are given below.

The position of a rotor binding site is given by

$$\theta_c = \theta + ia_0$$
$$r_c = 2 \, \text{nm},$$
$$z_c = 0.$$

Here $a_0 = 2\pi/n$ is the angular distance between two adjacent rotor sites, where n is the number of c subunits in the c ring.

For the F_1F_o complex, the position of the binding Na^+ ion at a rotor site is

$$\theta_p = \theta_c,$$
$$r_p = r_c + 0.3 \, \text{nm}.$$
$$z_p = z_c.$$

For the F_o motor (when the F_1 is absent), the position of the binding ion at a rotor site is

$$\theta_p = \theta_c + 0.2 \, a_0,$$
$$r_p, = r_c + 0.1 \, \text{nm},$$
$$z_p = z_c.$$

The stator channel lies within $[-0.6 \, a_0, -0.35 \, a_0]$.

By examining the experimental observations, it is not possible to assume there is one motor conformation with and without the membrane potential, and with and without the F_1 part.
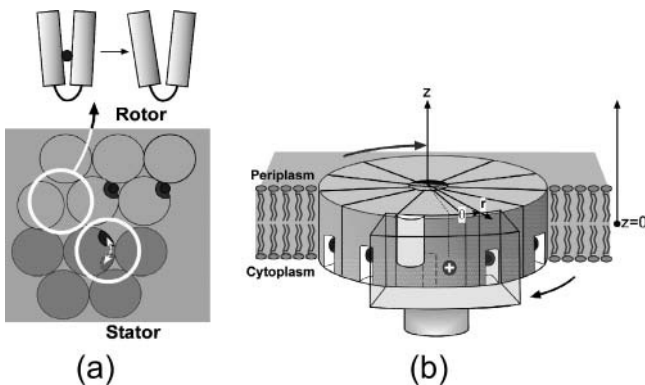
1. In the ATP synthesis direction, the stator charge is required to increase the ion dissociation rate through the rotor channel in region 3, but it should not affect the ion jump rates through the stator channel in region 2 significantly. On the other hand, ATP hydrolysis requires the stator charge to increase the ion dissociation rate through the stator channel in region 2, but have minimal effect on the ion jump rate through the rotor channel in region 3.
2. The $\Delta\psi$-driven ion uptake experiments with the wild-type F_o motor show that a membrane potential >40 mV is necessary. However, the maximum interaction energy between a 40 mV membrane potential and a rotor charge is $<2 \, k_B T$, too small to act as a switch. The problem is solved if one assumes that some protein rearrangement is induced by the membrane potential that slightly alters the position of the stator charge.
3. Ion exchange experiments suggest that without a membrane potential, a F_o motor is trapped in deep potential well, and is prevented from rotating in either direction. However, calculations show that a set of potentials preventing the F_o motor from rotating would result in too slow F_1-driven rotation.

To resolve these conflicting requirements on the rotor-stator interaction potentials, we must assume some slight membrane potential induced conformational changes. Since no detailed information on the conformational changes is available, a simple switching function of the membrane potential is used to connect different conformations,

$$f(\Delta\psi) = tanh(\Delta\psi/\Delta\psi_0), \tag{2}$$

where $\Delta\psi_0 = -100$ mV. The switching function changes the geometry parameters approximately linearly with small $\Delta\psi$, and approaches 1 for large values of $\Delta\psi$.

For the F_1F_o complex, the stator charge position is given by

$$\theta_q = -0.2 \, a_0 + 0.2 \, a_0 f(\Delta\psi),$$
$$r_q = 2.9 - 0.2 f(\Delta\psi) \, \text{nm},$$
$$z_q = 0.3 + 0.3 f(\Delta\psi) \, \text{nm}. \tag{3}$$

For the F_o motor (when the F_1 is absent), the stator charge position is given by

$$\theta_q = 0.15 \, a_0 + 0.5 \, a_0 f(\Delta\psi),$$
$$r_q = 2.7 + 0.3 f(\Delta\psi) \, \text{nm},$$
$$z_q = 0.5 + 0.3 f(\Delta\psi) \, \text{nm}. \tag{4}$$

An important feature of the model is that in some instances two consecutive rotor sites lie within the rotor-stator interface. In the corresponding two-channel model, the distance between the two stator half channels should be comparable to the distance between two rotor sites. This is reasonable: when an outer helix of the c subunit lies opposite helix IV of subunit a, the two rotor sites associated with the helix lie just at the two sides of helix IV of a.

Rotor-stator interactions

From structural information, we identify the following types of interactions:

1. Coulomb (electrostatic) interactions between the stator charge and the rotor charges, with and without the binding ions.
2. The horizontal component of membrane potential exerts an electrostatic force on unoccupied rotor sites. (This component must be present if the input channel is wholly, or partially, aqueous.)
3. The solvation energy experienced by an empty primary rotor site on entering the stator channel.
4. The steric interaction between rotor and stator that does not depend on the occupancy of the rotor sites.

FIGURE 8 (*a*) Proposed helix arrangement in the *a* subunit (see also Figs. 1 and 3). (*b*) The coordinate system adopted in this work.

Here we show how the full rotor-stator potentials were constructed with reference to the experimental observations. First, we examine the A mutant (Fig. 9 a).

a. For the A mutant, the electrostatic interaction is absent. The Na$^+$ dependence of ATP hydrolysis dictates an energy barrier to an empty rotor site in region 1. This barrier is also important for the A mutant to generate sufficient torque for ATP synthesis. The most likely origin of this barrier is from the outer α-helix of an empty rotor site that protrudes further toward the a subunit than that of an occupied site. This is consistent with the experimental finding that the rotor is stabilized by the binding ions (Meier and Dimroth, 2002). Since the rotor site must connect to the stator channel to allow ion passage, residue interactions between the a and c subunits may induce this deformation.

b. Ion concentration difference is not as effective as the membrane potential in driving the motor (Wehrle et al., 2002). Therefore, the rotor must be trapped in some potential wells. The sources of these potential wells are assigned to the nonspecific interactions between the rotor and stator; these include the hydrophobic and steric interactions between the stator and rotor that are independent of the chemical states of the rotor sites. The periodicity of the nonspecific interaction matches the symmetry of the rotor, and the magnitude is adjusted to allow the rotor to rotate barely without a membrane potential. This nonspecific interaction is experienced by the whole rotor. It can be treated equivalently by adding only one period of the term in Fig. 9, which shows single-site potentials.

c. In ATP synthesis direction, the horizontal component of the membrane potential pulls an empty rotor site toward the stator channel; this helps the rotor to overcome the potential barrier due to nonspecific interactions.

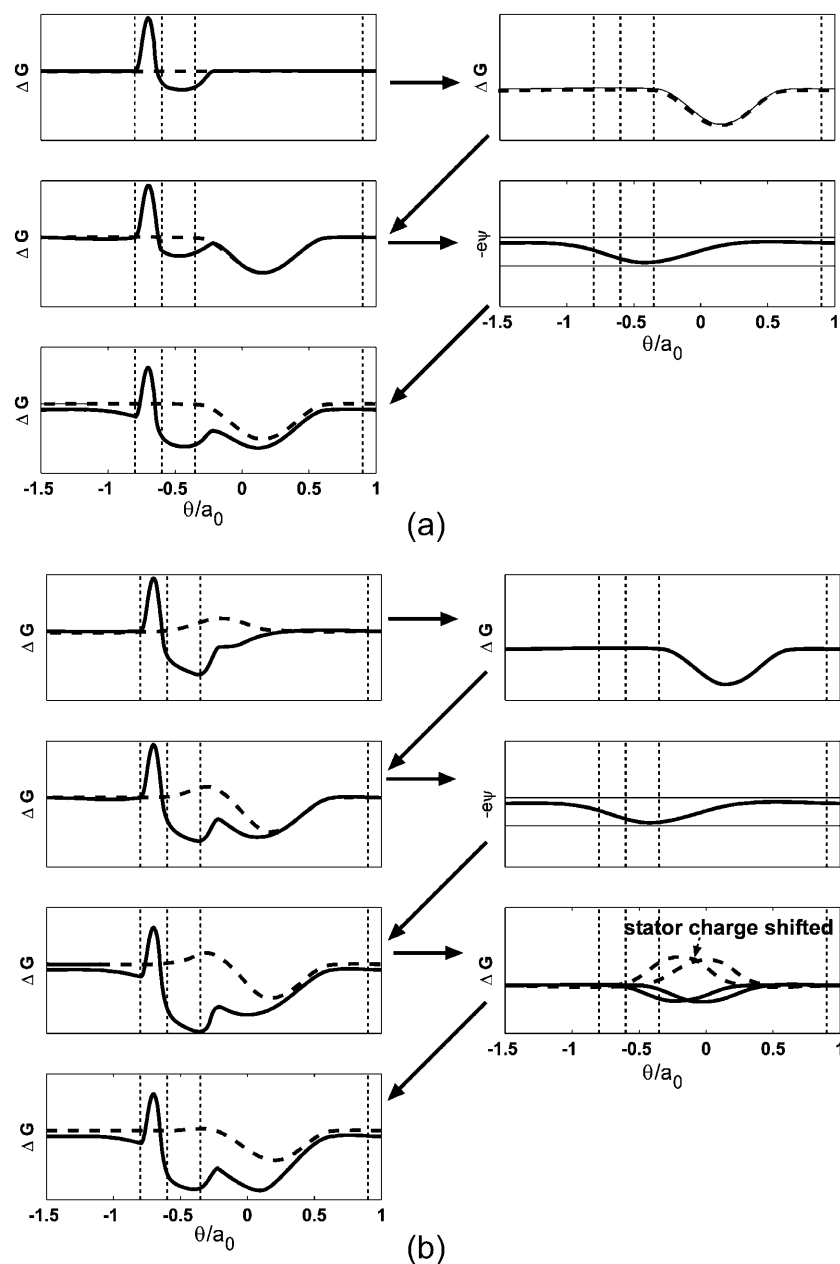Next, we consider the wild-type, and again begin with no membrane potential.

FIGURE 9   Step-by step construction of the free-energy profiles. (*a*) Mutant. (*b*) Wild-type.

a. The Coulomb interactions are present in this case. The empty site solvation remains. The stator charge position is tuned according to ATP hydrolysis experiments. Repulsion between the stator charge and an occupied rotor site prevents the latter moving from region 2 to region 3 without releasing its binding ion.

b. The nonspecific interaction and the steric barrier derived from the A mutant remain unchanged.

c. In ATP synthesis direction, the horizontal component of the membrane potential pulls an empty rotor site toward the stator channel. However, very high membrane potential would be required. Besides, the motor doesn't work well at high cytoplasmic sodium concentrations, since the stator charge is not in the position to knock out the binding ion of an incoming rotor site, which starts the power stroke to overcome the nonspecific potential barrier.

$$V_{ex}(\theta) = \begin{cases} -\dfrac{1}{2}V_1\{cos[2\pi(\theta - \theta_s)/(0.2\,a_0)] + 1\}, & \text{if } -0.8\,a_0 < \theta < -0.6\,a_0; \\ 0, & \text{otherwise.} \end{cases} \qquad (8)$$

d. This difficulty can be overcome if the membrane potential acts on the whole stator and changes stator conformation. Specifically, the stator charge is shifted slightly away from the stator channel. Vernier mismatch now ensures the two consecutive rotor sites cooperate in the ''pull-push'' manner emphasized in the article.

Mathematical modeling of rotor-stator interactions

By symmetry, only four rotor sites closest to the stator need be considered explicitly. The chemical state of a given binding site s_i is assigned a value 0 if empty and 1 if occupied. For bookkeeping reasons, the chemical states of the rotor are labeled as follows:

$$s = \begin{cases} \displaystyle\sum_{i=1}^{4} s_i 3^{4-i}, & \text{for ion exchange calculations} \\ \displaystyle\sum_{i=1}^{4} s_i 2^{4-i}, & \text{otherwise.} \end{cases} \qquad (5)$$

The rotor-stator interactions are periodic with period a_0. The periodicity imposes

$$V_s(\theta) = \sum_{i=1}^{3}[s_i V_o(\theta + (i-1)a_0) + (1 - s_i)V_e(\theta + (i-1)a_0)] + V_n(\theta), \qquad (6)$$

where $\theta \in [-2\,a_0, -a_0]$ is the angular coordinate of the leftmost rotor channel considered.

Nonspecific interactions

We model the nonspecific interaction term V_n by a cosine function with period a_0:

$$V_{sol}(\theta) = \begin{cases} -\dfrac{1}{2}V_1\{cos[2\pi(\theta - 0.45\,a_0)^2/(0.5\,a_0)^2] + 1\}, & \text{if } -0.7\,a_0 < \theta < -0.2\,a_0; \\ 0, & \text{otherwise.} \end{cases} \qquad (10)$$

$$V_n = -\frac{1}{2}V_0[\cos(2\pi(\theta - \theta_0)/a_0) + 1], \qquad (7)$$

where $V_0 = 10\,k_BT$, $\theta_0 = 0.15\,a_0$. The exact functional form of V_n is not significant, but the location of the minima affects the motor behavior.

The terms V_o and V_e refer to the interactions between the stator and an occupied (empty) rotor site. There are several contributions to these terms, which we describe separately.

The barrier in region 1

The necessary barrier of the empty state potential in region 1 is modeled by

Coulomb interactions

A major contribution to the total driving potential arises from the electrostatic interaction between the positive stator charge, q, and the rotor charges, q'. All charges were treated as effective point charges. A rotor binding site has charge $q' = -e$, and the ion on an occupied rotor site has $q = +e$. The major difference between an aR227A mutant and a wild-type motor is that the stator charge $q = 0$ for the former and $q' = 0.7\,e$ for the latter, if not otherwise specified. The charge-charge interaction is given by a shielded Coulomb interaction with a cutoff function

$$V_e = 56\,k_BT\frac{qq'}{\varepsilon d}\exp(-\lambda d)f(\theta), \qquad (9)$$

$$f(\theta) = \begin{cases} 1 - \exp(\alpha/\theta_{cut} - \alpha/\delta\theta^2) & \text{if } |\delta\theta| < \theta_{cut}, \\ 0 & \text{otherwise,} \end{cases}$$

where $\delta\theta = \theta_q - \theta_{q'}$, and $d = 0.5\,a_0$, is the charge-charge distance. The dielectric constant is taken as $\varepsilon = 4$, and the Debye shielding length is taken as $1/\lambda = 1.1$ nm, similar to the parameters used in Dimroth et al. (1999). There may be small Coulomb interactions between rotor binding sites. This mutual interference was not explicitly treated, but accounted for by the θ-dependent cutoff function, i.e., the rotor site interactions were treated as a background mean field. The cutoff distance was set at $\theta_{cut} = 0.5\,a_0$ so there would be no net Coulomb interaction between two neighboring rotor sites. The parameter $\alpha = 0.02/a_0^2$. Calculation results are not sensitive to the cutoff function.

Solvation energy

A rotor c site experiences nonuniform dielectric environment along the rotation path. On connecting to the aqueous stator channel, the free energy of an empty rotor c site can be lowered by forming hydrogen bonds. This solvation energy is modeled by

In the above formula, V_1 takes a value of 5 $k_B T$ and 9 $k_B T$ for the A mutant and wild-type, respectively. These values were chosen to fit the experimental data.

Membrane potential

The membrane potential along the middle of the membrane is nonuniform. Within region 2, the membrane potential is expected to take values close to the bulk membrane potential at the periplasm side, due to the existence of the aqueous stator channel and mobile ions. Similarly, outside region 2, the membrane potential is close to the cytoplasm side bulk value. By setting $\psi = 0$ at the cytoplasm side and $\psi = -\Delta\psi$ at the periplasm side, the membrane potential at the middle of the membrane experienced by a rotor site at position θ is modeled by

$$\psi_m = \begin{cases} (\psi_a - \psi_{mid})\{\exp[(\theta - \theta_a)^2 / \theta_\beta^2] - exp(-4)\} + \psi_{mid} & \text{if } |\theta - \theta_a| < 2\theta_\beta, \\ \psi_{mid} & \text{otherwise,} \end{cases} \quad (11)$$

where $\psi_a = -0.9 \, \Delta\psi$ is the membrane potential within the periplasm channel, $\psi_{mid} = -0.2 \, \Delta\psi$ is the membrane potential far away from the periplasm channel, $\theta_a = -0.4 \, a_0$ lies within the periplasm channel, and $\theta_\beta = 0.3 \, a_0$ is the effective length of the horizontal component of the membrane potential. The function form was chosen to approximately fit the results obtained by solving the Poisson equation with a crude model setup of a F_o motor. Then the electrostatic interaction between an empty rotor site and the membrane potential is $-e\psi_m$. The interaction for an occupied rotor site is neglected.

Transitions between chemical states modeled by Markov process

The intrinsic dissociation constant K_a of the rotor site along the stator channel is chosen to be 0.3 mM, as in the old model (Dimroth et al., 1999). Under the influence of the stator and the membrane potential, the jump rate constants of the sodium ions between the bulk in the periplasm side and a rotor binding site are given by

$$k_a^{on}(\theta) = 10^6 C_{Na^+}^{periplasm} h_a(\theta) \exp[\alpha(e\psi_p + V_e - V_o)],$$
$$k_a^{off}(\theta) = 10^6 h_a(\theta) \exp[-pK_a - (1-\alpha)(e\psi_p + V_e - V_o)]; \quad (12)$$

those between the cytoplasm side bulk and a rotor binding site are

$$k_c^{on}(\theta) = 10^6 C_{Na^+}^{cytoplasm} h_c(\theta) \exp[\alpha(e\psi_c + V_e - V_o)],$$
$$k_c^{off}(\theta) = 10^6 h_c(\theta) \exp[-pK_a - (1-\alpha)(e\psi_c + V_e - V_o)]. \quad (13)$$

The concentrations in the above expressions are in the unit of mole/liter; $\alpha = 0.3$, $\psi_p = -\Delta\psi$, and $\psi_c = 0$ are the electric potential on the periplasm and cytoplasm side, respectively. The function $h_a(\theta)$ takes value 1 within $[-0.6 \, a_0, -0.35 \, a_0]$, and 0 otherwise. The function $h_c(\theta)$ takes value 0 within $[-0.8 \, a_0, -0.05 \, a_0]$ and 1 otherwise. The overall transition matrix is $n \times n$, where $n = 81$ for ion exchange calculations, and 16 otherwise. An element of the transition matrix $K_{ij}(\theta)$ between two different rotor states $i \neq j$ is nonzero only if the two states are connected by one jump of a sodium ion, and the diagonal elements are given by

$$K_{ii} = \sum_{j \neq i} -K_{ij}(\theta).$$

Solving the Fokker-Planck equations

Dynamics of the system is described by a set of coupled Fokker-Planck equations,

$$\frac{\partial \rho_s(\theta)}{\partial t} = -D \frac{\partial}{\partial \theta} \left\{ \frac{1}{k_B T} \left[\frac{\partial V_s(\theta)}{\partial \theta} - \tau_L \right] \rho_s(\theta) + \frac{\partial \rho_s(\theta)}{\partial \theta} \right\} + \sum_{s'} K_{ss'}(\theta) \rho_{s'}(\theta), \quad (14)$$

with the diffusion constant $D = 5 \times 10^3 \, s^{-1}$.

All the results reported in this article are derived from the steady-state solutions, obtained by setting the left side of the above Fokker-Planck equations to zero. The numerical algorithm developed by Wang et al. (2003) was implemented to solve the equations. Periodic boundary conditions were used in all calculations. Rotation results were obtained by solving the coupled Fokker-Planck equations for the four rotor channels explicitly considered. Ion exchange calculations were performed by treating the Na^+ and $^{22}Na^+$ as two different species. Every binding site has three states: empty, Na^+ occupied, or $^{22}Na^+$ occupied. Thus there are $3^4 = 81$ states, so that the results were obtained by solving 81 coupled Fokker-Planck equations.

A summary of the parameter values used in the model is given in Table 2.

Additional results

Ratchet potential

In our previous model (Dimroth et al., 1999) a potential barrier in region 1 was introduced that acted as a ratchet potential (Peskin et al., 1993). At very low cytoplasmic Na^+ concentrations, a rotor site leaves region 1 and immediately releases its ion. The barrier prevents the empty rotor site from moving back into the rotor-stator interface. However, under physiological conditions, the cytoplasmic Na^+ concentration is much higher than the dissociation constant of the rotor site. Thus a rotor site keeps its binding ion until it is dissociated by the stator charge after one full rotation. Thus the potential barrier in region 1 no longer serves as a ratchet potential.

In this model, the ratchet potential is provided by the solvation well experienced by a negatively charged empty rotor site when it enters region 2. As discussed in the article, this solvation energy term is consistent with the observations by Junge and co-workers (Cherepanov et al., 1999). The F_o motor described here can synthesize ATP at both low and high ion concentrations, as required by the experimental findings. Calculations show that the absence of this ratchet potential impedes ATP synthesis function of the F_o motor.

The potential barrier in region 1 is required to explain the Na^+ requirement for ATP-driven rotation. Calculations performed without the barrier reduced the rotation rate significantly at very low cytoplasmic Na^+ concentrations, but had negligible effect at high Na^+ concentrations.

Coulomb interactions

In the ATP synthesis direction, an empty rotor must escape from the Coulomb potential well of the stator charge. If the rotor-stator Coulomb interaction is too large or too localized, it impedes motor rotation. The stator charge arises from a protonated amino acid residue. The charge is determined by the bulk pH and the acid dissociation constant K_a: $q = [H^+]/(K_a + [H^+])$. Strictly speaking, the dissociation constant—and

therefore the stator charge—is not constant in θ since an approaching rotor site will perturb the dissociation equilibrium. In addition, the stator charge is not a point, but is distributed over a small region; however, we have treated the stator charge as if it were an effective point charge whose value depends on the charge distribution. Fig. 10 shows the calculated rotational rates by varying the stator charge value. The rotation rate has a maximum at $q \approx 0.7$ e. This agrees with the experimental findings of Wehrle et al. (2002). In all subsequent calculations, we use this optimum charge value.

The F_o motor without membrane potential nor F_1

As shown in Fig. 11, *top panel*, an F_o motor with the aR227A mutation shows ion uptake at low internal Na^+ concentrations. The ion uptake is due to slow rotation driven by the difference in Na^+ concentration. Rotation and Na^+ uptake stops when the internal Na^+ concentration is comparable to the dissociation constant of the rotor site. On the other hand, introducing the stator charge traps the rotor in deep potential wells (due to combined interaction of Coulomb interactions of the stator charge, solvation energy, and the nonspecific interactions), so that no rotation can take place. Instead, a rotor site, once occupied, can rock back and forth through region 1, shuttling Na^+ ions between the two sides of the membrane (Kluge et al., 1992; Wehrle et al., 2002) (this is illustrated by movies provided also in the Supplementary Material).

When a small membrane potential is applied in either direction, the stator deforms slightly, altering the Coulomb and nonspecific interactions. This moves the minimum of the Coulomb potential from the valley of the steric potential to near its peak. Thus an empty rotor site attempting to access the stator channel sees a smaller potential barrier. Consequently, the rotor can rotate in either direction, depending on the direction of the applied membrane potential. Fig. 11, *bottom panel*, compares the experimental results with the computed ion uptake rate of the wild-type F_o motor as a function of the membrane potential (positive on the outside) (Kluge et al., 1992). Since the absolute values are unavailable, the experimental data were renormalized to fit the theoretical curve. One can see that the ion uptake rate increases dramatically after applying a membrane potential with magnitude >40 mV.

Reduction to a kinetic model

The Markov-Fokker-Planck (MFP) model presented here explicitly accounts for the rotational motion of the rotor. However, under certain circumstances,
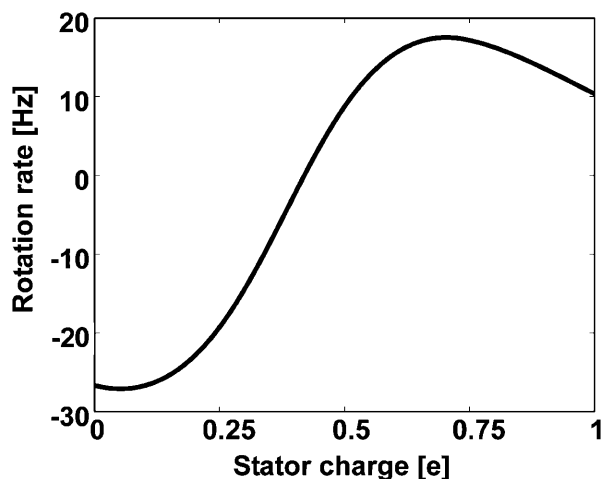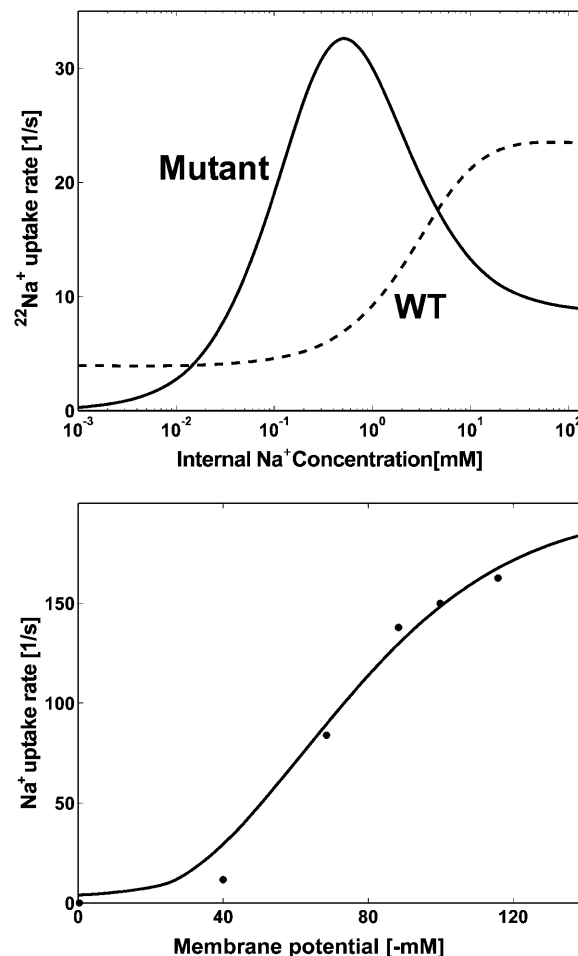

FIGURE 11 (*Top panel*) $^{22}Na^+$ uptake as a function of internal sodium concentration at $\Delta\psi = 0$. (*Solid line*) ΔpNa^+-driven uptake of the aR227A mutant. The external sodium concentration is 10 times higher than the internal concentration. (*Dashed line*) Ion exchange of the wild-type F_o motor. The external $^{22}Na^+$ concentration is 2 mM, and the stator charge is 0.7 e. (*Bottom panel*) The sodium uptake rate of a wild-type F_o motor as a function of the membrane potential, $\Delta\psi$. The uptake rate increases dramatically after applying a membrane potential with magnitude >40 mV.

it can be reduced to a purely kinetic model, which may be computationally more efficient.

At high (physiological) Na^+ ion concentrations, all the rotor sites except those two in contact with the stator are occupied with high probability. Therefore, the motor state can be represented by the four states of the two rotor sites in contact with the stator: (*EE, EO, OE, OO*), where E = empty and O = occupied. The reaction pathways are shown in Fig. 12, *left*. A typical cycle starts in the *OO* state, then switches to the *OE* state by relinquishing the bound ion at the right rotor site to the cytoplasm (under influence of the essential stator charge R227). The site then rotates into the stator input channel to become *EO*. There it picks up a Na^+ ion from the periplasm via the stator channel, triggering the transition back to the *OO* state, where the next occupied rotor site is ready to release its bound ion. To ensure that the rotor runs continuously without stalling, the distance between two neighboring rotor sites and the distance between the two ion jump regions must be about the same. This is easily satisfied, since both of them are expected to lie on the two sides of one alpha helix (Angevine and Fillingame, 2003; Angevine et al., 2003; Vonck et al., 2002). Note that in neither of the two potentials can the motor rotate freely. This is essential to

FIGURE 10 The rotation rate as a function of the stator charge. The optimum charge is about $q = 0.7$ e. The Na^+ concentrations are periplasm = 350 mM, cytoplasm = 50 mM, and $\Delta\psi = -200$ mV.
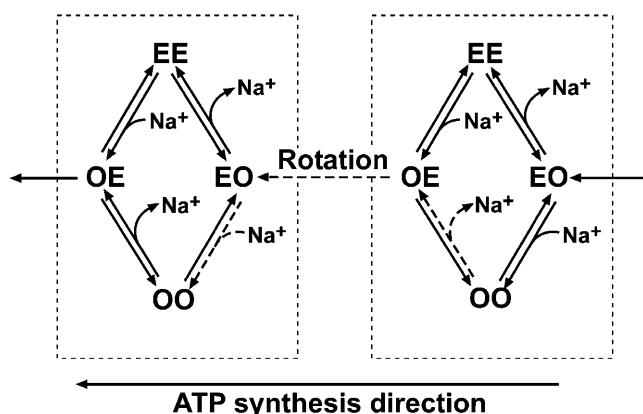
FIGURE 12 Approximate kinetic model at high cytoplasmic sodium concentrations. The dashed pathways show one ion passage cycle.

ensure tight coupling between chemical reactions and mechanical movement. The other pathway involving the *EE* state is similar.

The picture becomes more complicated at low Na^+ ion concentrations because the rotor cytoplasmic channels allow a rotor site to release its ion outside the rotor-stator interface. Consequently, more than four states are required to describe the system. At low ion concentrations, unidirectional rotation is ensured because, after leaving the rotor-stator interface, an occupied rotor site releases its binding ion and hydrates, preventing it from diffusing back into the hydrophobic rotor-stator interface. This is the ratchet mechanism proposed in an earlier model (Dimroth et al., 1999). However, at high (physiological) Na^+ concentrations, the binding ion remains on the rotor site until it makes a complete rotation and approaches the stator charge R227 from the opposite side of the stator. Thus under normal operating conditions this ratchet step is irrelevant for rotation.

The approximate kinetic cycle in Fig. 12 resembles the minimal kinetic model used by Junge and co-workers to interpret their experimental results on the proton-driven F_o motor (Cherepanov et al., 1999; Feniouk et al., 2004), as well as an earlier model of the proton motor (Elston et al., 1998):

1. The mechanical rotation step $OE \rightarrow EO$ is slow.
2. The proton motor kinetic model requires the ion binding residues in the periplasm channel to have a higher pKa (~ 6.1) (i.e., weaker proton binding) than the cytoplasm channel (~ 10). In the sodium model the rotor channels replace the stator cytoplasm channel, but have the same requirement on the relative binding strength: the stator periplasm channel is more hydrophilic (aqueous) than the cytoplasmic channels.
3. Most of the membrane potential drop takes place horizontally. Physically this is due to the highly nonuniform dielectric distribution of the rotor and stator within the membrane (Angevine and Fillingame, 2003; Angevine et al., 2003).

Therefore, the kinetic model and MFP models are complementary in describing the F_o motor. The kinetic model gives a simpler picture of the essential physics. Our model reveals connection between dynamics and motor structures (e.g., the function of the stator charge R227), provides more details to explain a large body of experimental observations, and demonstrates validity of the kinetic model. There are some subtle differences between the two pictures:

1. The kinetic model assumes some ''relay'' residues inside the two half channels, and implicitly assumes the ion jump process between the relay residues and the rotor site is very fast. In our model, we treat ion jumps as a one-step process between the bulk and the rotor site (i.e., all the intermediates are short-lived). The difference has little effect on the mathematical model, but requires a different structural interpretation.

2. The experimental observation that membrane potential $> \sim 40$ mV is necessary for rotation of the sodium motor required that we introduce a stator conformational change that shifted the location of the stator charge. Below this threshold, the potential barrier of the $EO \rightarrow OE$ rotation step is much too large to allow rotation even with high ion motive force. Junge and co-workers found that the conductance of the proton F_o motor is ohmic, so that there is no voltage threshold. This contradicts the observations of the Dimroth lab (Kaim and Dimroth, 1998b). Further experiments are necessary to clarify this difference between the two motors. Although a stator conformational change is necessary to model the observed voltage gating in the sodium motor, this difference from the proton motor does not affect the basic principle driving the F_o rotation mechanism.
3. In the sodium motor, rotor channels replace the cytoplasm half channel in the kinetic model. Consequently, some complexity appears at very low (but biologically insignificant) ion concentrations. There is debate in the literature on whether the cytoplasm half channel is provided by the rotor or the stator, or the stator-rotor interface—the so-called one-channel versus two-channel model (Angevine and Fillingame, 2003; Angevine et al., 2003). As pointed out in this article, at physiological conditions, the operating principle and dynamical performance of these two models are indistinguishable.
4. In the minimal kinetic model, mechanical rotation is assigned solely to the $OE \rightarrow EO$ transition, whereas in the MFP model, part of the mechanical rotation is performed by steps other than the $OE \rightarrow EO$ transition. This does not change the overall physical picture.

Thus the operating principle of the sodium and proton motors are the same, although there are differences in structural details. These differences cannot be discriminated at the level of the mesoscopic model presented herein.

SUPPLEMENTARY MATERIAL

An online supplement to this article can be found by visiting BJ Online at http://www.biophysj.org.

REFERENCES

Aksimentiev, A., I. Blabin, R. Fillingame, and K. Schulten. 2004. Insights into the molecular mechanism of rotation in the Fo sector of ATP synthase. *Biophys. J.* 86:1332–1344.

Angevine, C., and R. Fillingame. 2003. Aqueous access channels in subunit a of rotary ATP synthase. *J. Biol. Chem.* 278:6066–6074.

Angevine, C. M., K. A. G. Herold, and R. Fillingame. 2003. Aqueous access pathways in subunit a of rotary ATP synthase extend to both sides of the membrane. *Proc. Natl. Acad. Sci. USA.* 100:13179–13183.

Berg, H. C. 2003. The rotary motor of bacterial flagella. *Annu. Rev. Biochem.* 72:19–54.

Cherepanov, D., A. Mulkidjanian, and W. Junge. 1999. Transient accumulation of elastic energy in proton translocating ATP synthase. *FEBS Lett.* 449:1–6.

DeLeon-Rangel, J., D. Zhang, and S. Vik. 2003. The role of transmembrane span 2 in the structure and function of subunit a of the ATP synthase from *Escherichia coli. Arch. Biochem. Biophys.* 418:55–62.

Dimroth, P., H. Wang, M. Grabe, and G. Oster. 1999. Energy transduction in the sodium F-ATPase of *Propionigenium modestum*. *Proc. Natl. Acad. Sci. USA*. 96:4924–4929.

Dmitriev, O., P. Jones, and R. Fillingame. 1999. Structure of the subunit c oligomer in the F_1F_0 ATP synthase: Model derived from solution structure of the monomer and cross-linking in the native enzyme. *Proc. Natl. Acad. Sci. USA*. 96:7785–7790.

Elston, T., H. Wang, and G. Oster. 1998. Energy transduction in ATP synthase. *Nature*. 391:510–514.

Feniouk, B. A., M. A. Kozlova, D. A. Knorre, D. A. Cherepanov, A. Y. Mulkidjanian, and W. Junge. 2004. The proton driven rotor of ATP synthase: Ohmic conductance (10 fS), and absence of voltage gating. *Biophys. J.* 86:4094–4109.

Fung, D., and H. Berg. 1995. Powering the flagellar motor of *Escherichia coli* with an external voltage source. *Nature*. 375:809–812.

Grabe, M., H. Wang, and G. Oster. 2000. The mechanochemistry of the V-ATPase proton pumps. *Biophys. J.* 78:2798–2813.

Gräber, P., E. Schlodder, and H. T. Witt. 1977. Conformational change of the chloroplast ATPase induced by a transmembrane electric field and its correlation to phosphorylation. *Biochim. Biophys. Acta*. 3:426–440.

Grote, R. F., and J. T. Hynes. 1980. The stable states picture of chemical-reactions 2: rate constants for condensed and gas-phase reaction models. *J. Chem. Phys.* 73:2715–2732.

Jiang, W., and R. Fillingame. 1998. Interacting helical faces of subunits a and c in the F_1F_0 ATP synthase of *Escherichia coli* defined by disulfide cross-linking. *Proc. Natl. Acad. Sci. USA*. 95:6607–6612.

Junge, W. 1970. Critical electric potential difference for photophosphorylation. Its relation to the chemiosmotic hypothesis and to the triggering requirements of the ATPase system. *Eur. J. Biochem.* 14:582–592.

Junge, W. 1999. ATP synthase and other motor proteins. *Proc. Natl. Acad. Sci. USA*. 96:4735–4737.

Kaim, G., and P. Dimroth. 1998a. A triple mutation in the a subunit of the *Escherichia coli/Propionigenium modestum* F_1F_0 ATPase hybrid causes a switch from Na^+ stimulation to Na^+ inhibition. *Biochemistry*. 37:4626–4634.

Kaim, G., and P. Dimroth. 1998b. Voltage-generated torque drives the motor of the ATP synthase. *EMBO J.* 17:5887–5895.

Kaim, G., and P. Dimroth. 1999. ATP synthesis by F-type ATP synthase is obligatorily dependent on the transmembrane voltage. *EMBO J.* 18:4118–4127.

Kaim, G., M. Prummer, B. Sick, G. Zumofen, A. Renn, U. P. Wild, and P. Dimroth. 2002. Coupled rotation within single F0F1 enzyme complexes during ATP synthesis or hydrolysis. *FEBS Lett.* 525:156–163.

Kluge, C., and P. Dimroth. 1992. Studies on Na^+ and H^+ translocation through the F_0 part of the Na^+-translocating F_1F_0 ATPase from *Propionigenium modestum*: discovery of a membrane potential dependent step. *Biochemistry*. 31:12665–12672.

Kluge, C., W. Laubinger, and P. Dimroth. 1992. The Na(+)-translocating ATPase of *Propionigenium modestum*. *Biochem. Soc. Trans.* 20:572–577.

Laubinger, W., and P. Dimroth. 1987. Characterization of the Na^+-stimulated ATPase of *Propeonigenium modestum* as an enzyme of the F_1F_0 type. *Eur. J. Biochem.* 168:475–480.

Laubinger, W., and P. Dimroth. 1988. Characterization of the ATP synthase of *Propeonigenium modestum* as a primary sodium pump. *Biochemistry*. 27:7531–7537.

Meier, T., and P. Dimroth. 2002. Intersubunit bridging by sodium ions as rationale for the unusual stability of Na^+-F_1F_0 synthase. *EMBO Rep.* 3:1094–1098.

Meier, T., U. Matthey, C. von Ballmoos, J. Vonck, T. K. von Nidda, W. Kühlbrandt, and P. Dimroth. 2002. Evidence for structural integrity in the undecameric c-rings isolated from sodium ATP synthases. *J. Mol. Biol.* 203:389–397.

Mellwig, C., and B. Bottcher. 2003. A unique resting position of the ATP-synthase from chloroplasts. *J. Biol. Chem.* 278:18544–18549.

Oster, G., and H. Wang. 2003. Rotary protein motors. *Trends Cell Biol.* 13:114–121.

Pedersen, P., Y. H. Ko, and S. Hong. 2000. ATP synthases in the Year 2000: evolving views about the structures of these remarkable enzyme complexes. *J. Bioenerg. Biomembr.* 32:325–332.

Peskin, C. S., G. M. Odell, and G. Oster. 1993. Cellular motions and thermal fluctuations: the Brownian ratchet. *Biophys. J.* 65:316–324.

Rastogi, V., and M. Girvin. 1999. Structural changes linked to proton translocation by subunit c of the ATP synthase. *Nature*. 402:263–268.

Rubinstein, J. L., J. E. Walker, and R. Henderson. 2003. Structure of the mitochondrial ATP synthase by electron cryomicroscopy. *EMBO J.* 22:6182–6192.

Schlodder, E., M. Rogner, and H. T. Witt. 1982. ATP synthesis in chloroplasts induced by a transmembrane electric potential difference as a function of the proton concentration. *FEBS Lett.* 138:13–18.

Schlodder, E., and H. T. Witt. 1980. Electrochromic absorption changes of a chloroplast suspension induced by an external electric field. *FEBS Lett.* 112:105–113.

Schlodder, E., and H. T. Witt. 1981. Relation between the initial kinetics of ATP synthesis and of conformational changes in the chloroplast ATPase studied by external field pulses. *Biochim. Biophys. Acta*. 635:571–584.

Vinogradov, A. D. 2000. Steady-state and pre-steady-state kinetics of the mitochondrial F_1F_0 ATPase: is ATP synthase a reversible molecular machine? *J. Exp. Biol.* 203:41–49.

von Ballmoos, C., Y. Appoldt, J. Brunner, T. Granier, A. Vasella, and P. Dimroth. 2002a. Membrane topography of the coupling ion binding site in Na^+ translocating F_1F_0 ATP synthase. *J. Biol. Chem.* 277:3504–3510.

von Ballmoos, C., T. Meier, and P. Dimroth. 2002b. Membrane embedded location of Na+ or H+ binding sites on the rotor ring of F1F0 ATP synthase. *Eur. J. Biochem.* 269:5581–5589.

Vonck, J., T. K. von Nidda, T. Meier, U. Matthey, D. Mills, W. Kühlbrandt, and P. Dimroth. 2002. Molecular architecture of the undecameric rotor of a bacterial Na^+-ATP synthase. *J. Mol. Biol.* 321:307–316.

Wang, H., and G. Oster. 2001. Ratchets, power strokes, and molecular motors. *Applied Physics A.* 75:315–323.

Wang, H., C. Peskin, and T. Elston. 2003. A robust numerical algorithm for studying biomolecular transport processes. *J. Theor. Biol.* 221:491–511.

Wehrle, F., G. Kaim, and P. Dimroth. 2002. Molecular mechanism of the ATP synthase's F_0 motor probed by mutational analyses of subunit a. *J. Mol. Biol.* 322:369–381.